



DØnote 5262-CONF

Measurement of the top-antitop quark pair production cross section in proton-antiproton collisions at $\sqrt{s} = 1.96$ TeV in the lepton+jets final state using event kinematics on 900 pb^{-1} of DØ data

The DØ Collaboration
URL: <http://www-d0.fnal.gov>
(Dated: October 30, 2006)

We present a preliminary measurement of the top-antitop quark pair ($t\bar{t}$) production cross section in proton-antiproton collisions at $\sqrt{s} = 1.96$ TeV by applying a topological discriminant to events with e +jets or μ +jets final states. This analysis utilizes an integrated luminosity of 913 pb^{-1} in e +jets channel and 871 pb^{-1} in μ +jets channel collected by the DØ detector at the Fermilab Tevatron. Assuming a top quark mass of $175 \text{ GeV}/c^2$, we measure:

$$\begin{aligned}\sigma_{p\bar{p} \rightarrow t\bar{t}+X} &= 6.6_{-1.1}^{+1.2} \text{ (stat)} \pm 0.8 \text{ (syst)} \pm 0.4 \text{ (lumi)} \text{ pb} \quad (\text{in the } e\text{-jets channel}) \\ \sigma_{p\bar{p} \rightarrow t\bar{t}+X} &= 5.9_{-1.2}^{+1.3} \text{ (stat)} \pm 0.8_{-0.8}^{+0.9} \text{ (syst)} \pm 0.4 \text{ (lumi)} \text{ pb} \quad (\text{in the } \mu\text{-jets channel}) \\ \sigma_{p\bar{p} \rightarrow t\bar{t}+X} &= 6.3_{-0.8}^{+0.9} \text{ (stat)} \pm 0.7 \text{ (syst)} \pm 0.4 \text{ (lumi)} \text{ pb} \quad (\text{both channels combined}).\end{aligned}$$

Preliminary Results for Fall 2006 Conferences

I. INTRODUCTION

We study top-antitop quark pair production in proton-antiproton collisions at $\sqrt{s} = 1.96$ TeV. In the Standard Model, the decay channel $t \rightarrow Wb$ dominates the decay of top quarks. Depending on the decay of the W bosons to $\ell\nu$ or $q\bar{q}'$, top-antitop quark pairs can thus decay to final states containing two, one, or no charged leptons with corresponding neutrinos and a number of jets from the fragmentation of the b quarks and hadronic W boson decays. Here we measure the production cross section using the decay channel in which there is one leptonic and one hadronic W boson decay, resulting in final states with one charged lepton, also called the lepton+jets channel.

Theoretical calculations of the top-antitop quark production cross section predict $t\bar{t}$ cross section $\sigma_{t\bar{t}}$ of 6.8 ± 0.6 pb [1] and $6.7^{+0.7}_{-0.9}$ pb [2] at the next-to-next-to-leading order in perturbative QCD. The precise measurement of $\sigma_{t\bar{t}}$ is not only of interest as a test of perturbative QCD, but it also permits to probe the effects of new physics. Such effects could lead to a $t\bar{t}$ cross section dependence on the final state of the top quark pair. It is therefore necessary to measure $\sigma_{t\bar{t}}$ in all decay channels. A detailed study of top-antitop quark pair production demonstrates our understanding of the signal and the background processes in our data on which all our measurements of the properties of the top quark are based.

In this paper we report on preliminary results obtained from an analysis of about 900 pb^{-1} of data taken by the DØ detector during Run II. We carry out a preselection that selects events with the desired e +jets or μ +jets final state; the τ +jets channel therefore contributes through the leptonic τ decays. After the preselection the data are still dominated by backgrounds, mainly from W +jets production. For the resulting event sample we build a discriminant based on a number of variables that describes the kinematics of the events and allows us to separate the dominant W +jets background from the signal. We extract the top-antitop quark signal and the background contributions by performing a fit of the discriminant shapes for the signal and backgrounds to the discriminant distribution in data.

II. THE DØ DETECTOR

The DØ detector is a multipurpose collider detector [3]. The central tracker employs silicon microstrips close to the beam and concentric cylinders covered with scintillating fibers in a 2 T magnetic field parallel to the beam axis. The liquid-argon/uranium calorimeter is divided into a central section covering $|\eta| \leq 1.1$ and two endcap calorimeters extending coverage to $|\eta| \leq 4.2$ [4], where $\eta = -\ln[\tan(\theta/2)]$ and θ is the polar angle with respect to the proton beam direction. The muon spectrometer consists of a layer of drift chambers and scintillation counters between the calorimeter and 1.8 T toroidal magnets, followed by two similar layers outside the toroids.

III. PRESELECTION OF LEPTON+JETS EVENTS

The characteristic topology of the lepton+jets channel is one isolated lepton with high transverse momentum, large \cancel{E}_T due to the undetected neutrino and four or more jets with high transverse momentum. The preselection is designed to define a data sample enriched in W +jets and top events. To ensure that the e +jets and μ +jets topological analyses are orthogonal to each other and to the dilepton analyses, events with a second lepton with high transverse momentum are explicitly vetoed.

The following requirements are imposed to preselect the data samples in both the e +jets and the μ +jets channel:

- primary event vertex with $|z| \leq 60$ cm and at least 3 tracks attached;
- four or more jets with $p_T > 20$ GeV/ c and $|\eta| < 2.5$;
- $\cancel{E}_T > 20$ GeV.

The following requirements are imposed to preselect the data sample in the e +jets channel:

- one isolated electron with $p_T > 20$ GeV/ c and $|\eta| < 1.1$ that originates from the primary vertex;
- $\Delta\phi(e, \cancel{E}_T) > 0.7 \cdot \pi - 0.045 \cdot \cancel{E}_T$;
- no second isolated electron with $p_T > 15$ GeV/ c and $|\eta| < 2.5$;
- no isolated muon with $p_T > 15$ GeV/ c and $|\eta| < 2.0$.

The following requirements are imposed to preselect the data sample in the μ +jets channel:

- one isolated muon with $p_T > 20$ GeV/ c and $|\eta| < 2.0$ that originates from the primary vertex;
- $\Delta\phi(e, \cancel{E}_T) > 0.48 \cdot \pi - 0.033 \cdot \cancel{E}_T$;
- invariant mass of the selected muon and any other muon $m_{\mu\mu} < 70$ GeV/ c^2 or $m_{\mu\mu} > 110$ GeV/ c^2 to reject $Z(\rightarrow \mu\mu)$ +jets events;
- no isolated electron with $p_T > 15$ GeV/ c and $|\eta| < 2.5$;
- no second isolated muon with $p_T > 15$ GeV/ c and $|\eta| < 2.0$.

The objects used in this selection can be described as follows:

The **primary event vertex** defines the position of the hard proton-antiproton interaction in the detector and is the reference point for the calculation of kinematic variables, such as transverse momenta.

Electrons are clusters of energy depositions with at least 90% of their energy in the electromagnetic section of the calorimeter. The profile of the clusters must be consistent in shape with an electromagnetic shower profile predicted by simulation. The cluster must be isolated from other energy deposits in the calorimeter: the fraction of energy in an annular isolation cone of radius $0.2 < R = \sqrt{\Delta\phi^2 + \Delta\eta^2} < 0.4$ must be less than 15% of the energy in the core cone of radius $R < 0.2$. Every electron must be matched with a charged particle track from the tracking detectors with $p_T > 5$ GeV/ c . Finally, the electron must be consistent with the expectations for a prompt high- p_T isolated electron based on a discriminant combining information both from the central tracking system and the calorimeter.

Muons are reconstructed primarily as tracks in the muon spectrometer. We accept muons with $|\eta| < 2$. They must have matched track segments in muon drift chambers inside and outside the toroid magnet. We reject cosmic rays by requiring the time of hits in the muon scintillation counters to be within 10 ns of the beam crossing time. The track reconstructed in the muon system must match a track reconstructed in the central tracker. The central detector track must have a good quality and a distance of closest approach to the beam line in the transverse plane of less than 0.02 cm if it has hits in the silicon tracker or < 0.2 cm if it does not. Muons must be separated from jets by $\Delta R = \sqrt{\Delta\eta^2 + \Delta\phi^2} > 0.5$. For additional isolation, we require that the energy measured by the calorimeter in an annular cone of radius $0.1 < R < 0.4$ around the muon direction must be less than 8% of the muon p_T and the momenta of all tracks in a cone of radius $R < 0.5$ around the muon direction, except the track matched to the muon, must add up to less than 6% of the muon p_T .

Jets are reconstructed from energy deposits in the calorimeter using the Run 2 cone algorithm [5]. To eliminate jets seeded by calorimeter noise, the following quality criteria are applied: The energy in the electromagnetic section of the calorimeter must be greater than 5% and less than 95% of the total jet energy. The energy in the coarse hadronic calorimeter must be less than 40% of the total jet energy. The ratio of the highest to the second highest cell in transverse energy must be less than 10. No tower may contain more than 90% of the jet energy. The reconstructed jet must also be consistent with the information from the level 1 calorimeter trigger.

Neutrinos carry away energy that can be inferred using energy conservation in the transverse plane. The sum of the transverse energies of undetected neutrinos is equal to the negative sum of the transverse energies of all particles that were observed in the detector. In practice we compute the missing transverse energy by adding up vectorially the transverse energies in all cells of the electromagnetic and fine hadronic calorimeters. Cells in the coarse hadronic calorimeter are added only if they are part of a good jet. This raw quantity is then corrected for the energy corrections applied to the reconstructed objects and for the momentum of all muons in the event, corrected for their energy loss in the calorimeter.

Table I shows the preselection efficiencies, numbers of events selected and integrated luminosities for the two channels. The efficiencies for the preselection of $t\bar{t}$ events are measured in $t\bar{t}$ Monte Carlo simulation with respect to $t\bar{t} \rightarrow \ell\nu_\ell q\bar{q}'b\bar{b}$, where ℓ can be an electron or muon from the decay of a W boson, including $W \rightarrow \tau\nu$ decays. The total efficiencies are corrected for trigger efficiencies and for differences between the Monte Carlo simulation and the collider data by applying scale factors.

IV. BACKGROUNDS

The selected samples contain two major sources of background: The dominant background is a physics background with the same signature as $t\bar{t}$ events, the production of W bosons in association with jets ($W + \text{jets}$), with the W boson decaying leptonically. The second major background is instrumental, originating from multijet events in which one of the jets is misidentified as an isolated electron or in which a muon appears isolated because the jet was not reconstructed. In both cases significant \cancel{E}_T arises from fluctuations and mismeasurements of the jet energies. In this case the missing transverse energy tends to be collinear with a reconstructed object (lepton or jet) in the event. We

	e +jets	μ +jets
preselection efficiency	14.04 ± 0.07	14.50 ± 0.07
trigger efficiency	96.65 ± 0.02	87.02 ± 0.06
data/MC correction	88.32 ± 0.02	90.09 ± 0.06
total efficiency	11.99 ± 0.06	11.40 ± 0.06
number of events selected	352	363
integrated luminosity	913 pb^{-1}	871 pb^{-1}

TABLE I: Summary of the preselection efficiencies and data/MC correction factors in %, using statistical uncertainties only.

suppress these background events by applying a cut on the azimuthal separation between \cancel{E}_T and the lepton without suffering from a large signal efficiency loss. “QCD” events are selected by using events with two or more jets and inverting lepton quality cuts. These events are dominated by background and Figure 1 illustrates that in these events, missing transverse energy tends to point along the leptons.

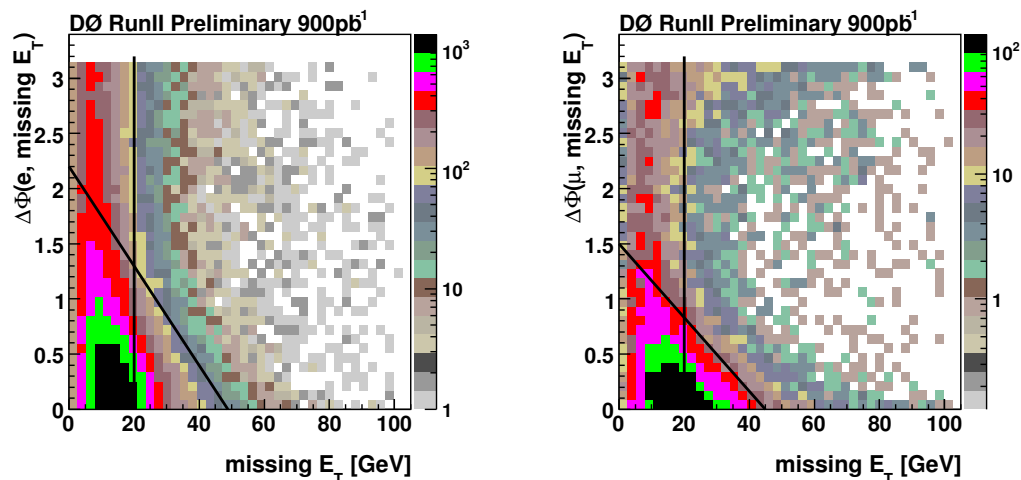


FIG. 1: Azimuthal separation between the isolated lepton and \cancel{E}_T for events with an electron (left) or a muon (right). The preselection was relaxed to include events with at least two jets in order to increase the number of events. To show a background dominated sample, lepton quality cuts have been inverted. Similar distributions are observed for other jet multiplicities.

We determine the instrumental background contamination directly from the data by using “loose” data samples for which the requirements for the isolated lepton were relaxed relative to the preselection described in section III. We determine the probability for an electron or muon that passes the loose selection cuts to also pass the full preselection cuts to be

$$\begin{aligned}\varepsilon_{sig} &= 83.8 \pm 1.0(stat) \pm 2.2(syst)\% \text{ for } e\text{-jet events,} \\ \varepsilon_{sig} &= 84.9 \pm 1.0(stat) \pm 2.0(syst)\% \text{ for } \mu\text{-jet events,}\end{aligned}$$

from simulated W +jets (using ALPGEN) and $t\bar{t}$ -events (using PYTHIA), corrected for data/MC differences. The probability that a misidentified isolated lepton in the loose sample also passes the full preselection cuts is

$$\begin{aligned}\varepsilon_{mis} &= 18 \pm 1(stat) \pm 3(syst)\% \text{ for } e\text{-jet events,} \\ \varepsilon_{mis} &= 24 \pm 1(stat) \pm 3(syst)\% \text{ for } \mu\text{-jet events,}\end{aligned}$$

as determined from the lepton+jets data directly. To select a sample that is dominated by misidentified leptons we use only events with low \cancel{E}_T to eliminate the W boson decays from the samples.

We can now relate the numbers of lepton candidates in the preselected samples due to genuine leptons (N_{sig}) and due to misidentified jets (N_{mis}) to the corresponding numbers in the loose samples using these efficiencies, which results in the following two equations:

$$\begin{aligned}N' &= N_{sig} + N_{mis} \\ N &= \varepsilon_{sig}N_{sig} + \varepsilon_{mis}N_{mis}.\end{aligned}$$

Here the total number of lepton candidates after full preselection is N and after loose preselection is N' . We can now solve this system of equations for N_{mis} and N_{sig} . For the preselected samples, Fig. 2 shows the resulting composition of the samples versus the W transverse mass computed from lepton p_T and \cancel{E}_T , using the above method to normalize $W + jets$ Monte Carlo and the multijet data contribution obtained from the dataset passing the loose but not the full preselection cuts. Table II lists the results.

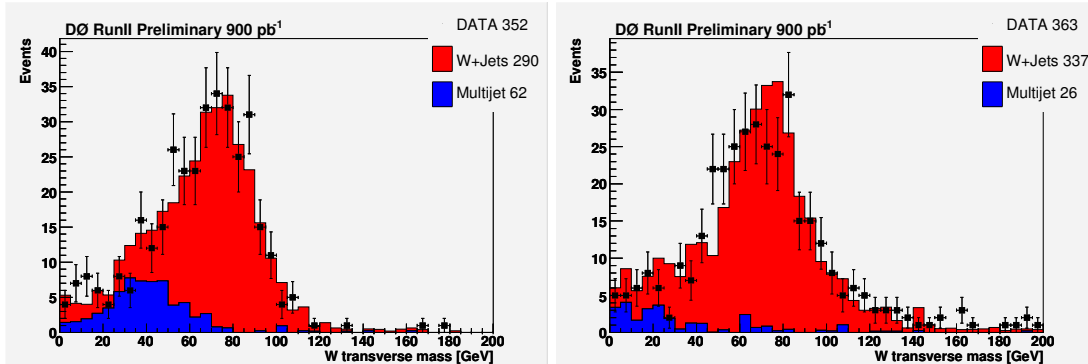


FIG. 2: W transverse mass distributions for the preselected e +jets (left) and μ +jets (right) sample with determined fractions of leptons from W boson decays and multijet background.

sample	N'	N	ε_{sig}	N_{sig}	ε_{mis}	N_{mis}	ε_{sig}	ε_{mis}
e +jets	689	352	290.4	61.6	0.84	0.18		
μ +jets	506	363	336.8	26.2	0.85	0.24		

TABLE II: Number of events in the loose and fully preselected samples and the expected contribution from leptons from W boson decays and multijet background.

V. TOPOLOGICAL DISCRIMINANT

The purpose of the preselection is to extract genuine lepton+jets events with maximum efficiency while rejecting background events with misidentified isolated leptons. We now have to determine how many of these events are from top-antitop quark pair production and how many are from W +jets production. We achieve this by evaluating a discriminant based on the ratio from six kinematical variables. The variables were chosen to construct a discriminant that provides maximal discrimination between signal and background while being minimally sensitive to systematic uncertainties such as the jet energy scale calibration.

The following six variables are used to construct the discriminant:

- H_T , given by the scalar sum of the p_T of the four leading jets.
- $\Delta\phi(\text{lepton}, \cancel{E}_T)$, the azimuthal opening angle between the lepton p_T and the missing p_T .
- $K_T^{min'}$ = $\min(\Delta R_{jj}) \min(p_T) / (p_T^{\text{lepton}} + \cancel{E}_T)$ provides a measure of the minimum relative jet p_T . $\min(\Delta R_{jj})$ corresponds to the minimum separation in $\eta - \phi$ space between any pair of jets and $\min(p_T)$ is the lesser jet p_T of that pair. In order to reduce the correlation of this variable with the jet energy scale, it is divided by another variable that has the same sensitivity.
- Centrality $\mathcal{C} = H_T/H$. H is the scalar sum of the energy of the jets.
- Aplanarity \mathcal{A} , a measure of the flatness of the event, is defined as $\mathcal{A} = \frac{3}{2}\lambda_3$, where λ_3 is the smallest eigenvalue of the normalized momentum tensor \mathcal{M} [6]. Therefore, it is defined in the range $0 \leq \mathcal{A} \leq 0.5$. Large values of \mathcal{A} are indicative of spherical events, whereas small values correspond to planar events.
- Sphericity \mathcal{S} of the event is defined as $\mathcal{S} = \frac{3}{2}(\lambda_2 + \lambda_3)$, where λ_2 and λ_3 are the smallest eigenvalues of the normalized momentum tensor \mathcal{M} [6], so that $0 \leq \mathcal{S} \leq 1$. Sphericity is a measure of the summed p_{\perp}^2 with respect to the event axis; a 2-jet event corresponds to $\mathcal{S} \approx 0$ and an isotropic event to $\mathcal{S} \approx 1$.

Only the four leading jets are used to determine the topological variables. This does not reduce the statistical separation power, but it reduces the dependence on systematic effects on the modeling of soft radiation (like underlying event, initial state radiation via parton shower, etc). The normalized distributions of the six topological variables are shown in Figs. 3 and 4.

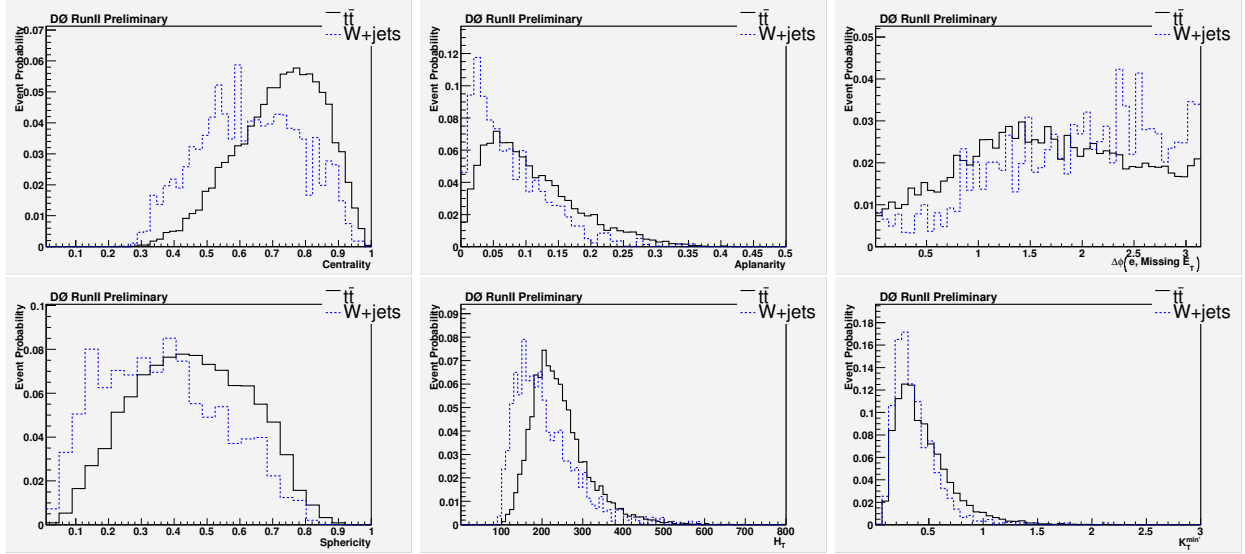


FIG. 3: Likelihood input distributions for top-antitop quark pair production and W +jets production for the e +jets channel.

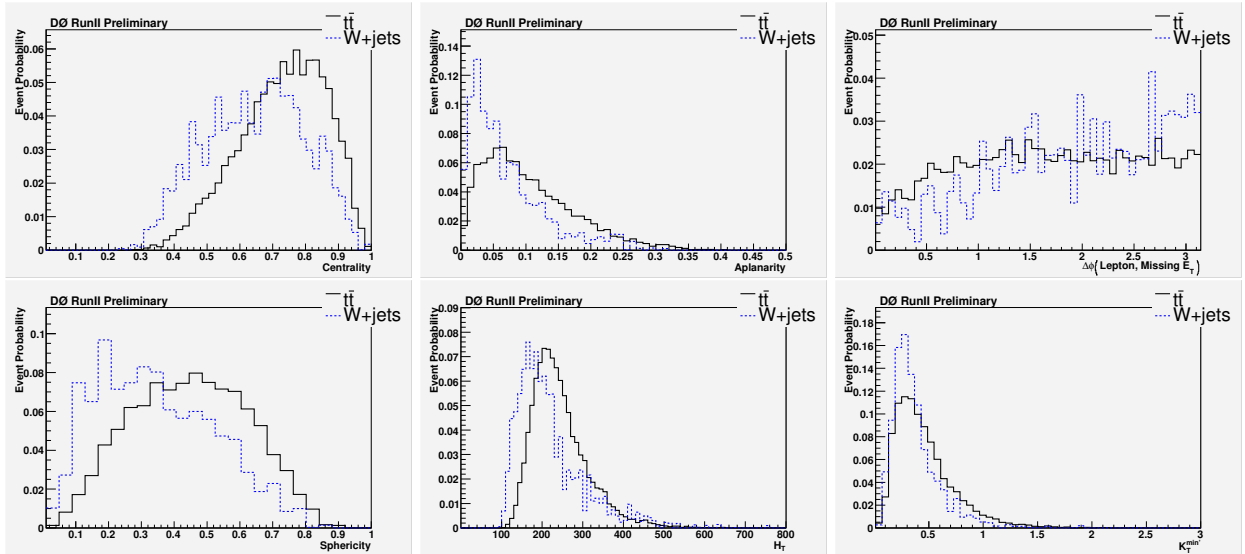


FIG. 4: Likelihood input distributions for top-antitop quark pair production and W +jets production for the μ +jets channel.

We observe that the kinematic properties of the multijet and W +jets background events are similar enough that we can use the discriminant function obtained from the simulated W +jets for both background sources.

We compute the ratio of the normalized distributions of each of these variables for signal and background. To smooth out the distributions, we fit the logarithm of this ratio with a polynomial. For each event we evaluate the polynomial fit to determine the value of the ratio $\ln S/B$. We then combine these ratios for the six individual variables into a discriminant function defined as

$$\mathcal{D} = \frac{\exp(\sum_i (\ln \frac{S}{B})_i)}{\exp(\sum_i (\ln \frac{S}{B})_i) + 1}.$$

The resulting discriminants from top-antitop quark pair production, W +jets simulations and multijet backgrounds are shown in Fig. 5.

We now fit the distribution of the likelihood discriminant for the e +jets and μ +jets data samples with these three components. In this fit we constrain the ratio of events with leptons from W boson decays and multijet background to the ratio determined using the procedure described in section IV. A small ($\approx 2\%$) contribution from the $t\bar{t}$ events with two leptons in the final state is considered to be a part of the signal.

The input values for the likelihood fits are summarised in Table III. The results of the likelihood fits are shown in Fig. 6. Table IV summarizes the fitted number of events and corresponding fractions of signal and backgrounds

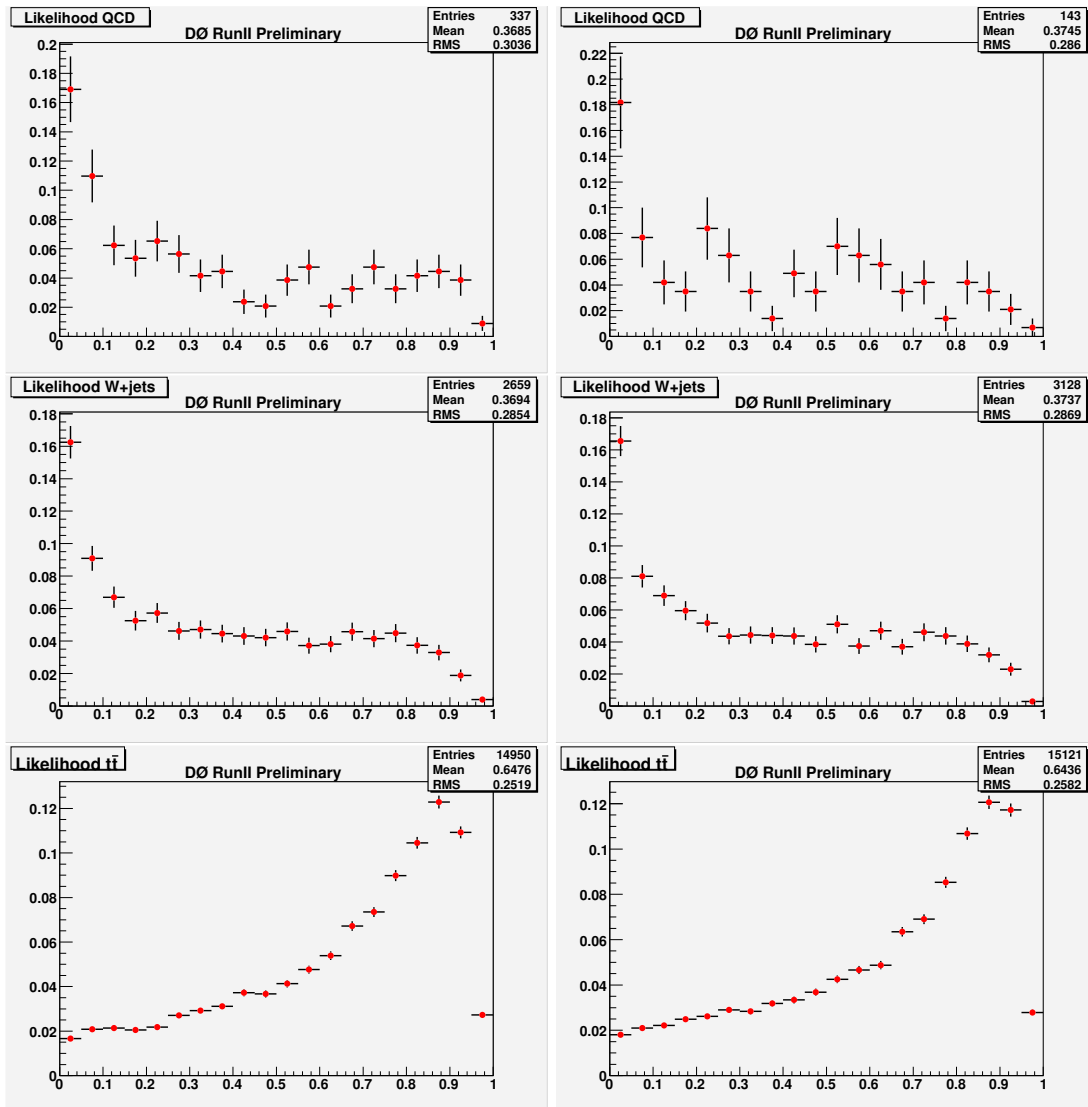


FIG. 5: Likelihood discriminant distributions for multijet backgrounds, W +jets production and top-antitop quark pair production for e +jets events (left) and μ +jets events (right).

	N'	N	\mathcal{B}	$\int \mathcal{L} dt$ (pb $^{-1}$)	ε	ε_{sig}	ε_{mis}
e +jets	689	352	0.17	913	0.12	0.84	0.18
μ +jets	506	363	0.17	871	0.11	0.85	0.24

TABLE III: Inputs for the likelihood discriminant fits.

	$N^{t\bar{t}}$	N^{W+jets}	$N^{multijet}$	$f^{t\bar{t}}$ (%)	f^{W+jets} (%)	$f^{multijet}$ (%)
e +jets	124 ± 22	168 ± 25	62 ± 4	35 ± 6	48 ± 7	17 ± 1
μ +jets	100^{+22}_{-21}	236 ± 26	27 ± 4	28 ± 6	65 ± 7	7 ± 1

TABLE IV: Results of the likelihood fits.

in each channel.

Figures 11 and 12 show the distributions of likelihood input variables for data overlaid with the predicted distributions from the simulation, exhibiting reasonable agreement. Kolmogorov-Smirnov (KS) probabilities are given in upper center of each plot to quantify the agreement between the observed and predicted distributions.

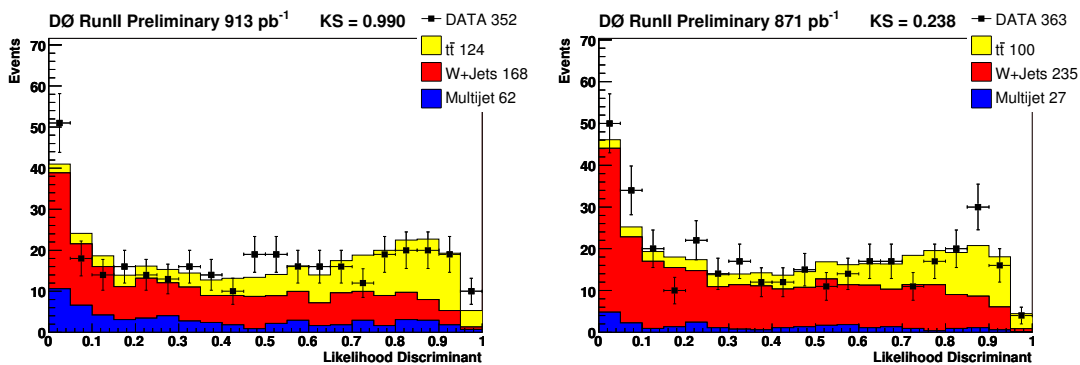


FIG. 6: Likelihood discriminant distribution for data overlaid with the result from the fit of top-antitop quark pair production, W +jets production and multijet jet background templates for e +jets events (left) and μ +jets events (right). The normalisation of each template is indicated in the legend.

VI. SYSTEMATIC UNCERTAINTIES

The systematic uncertainties can be subdivided into uncertainties on the preselection efficiency and uncertainties on the estimated number of signal events from the likelihood fit. Table V summarizes the size of all systematic uncertainties.

VII. RESULTS

The $t\bar{t}$ production cross section in the lepton+jets channel is given by:

$$\sigma = \frac{N^{t\bar{t}}}{B \cdot \mathcal{L} \cdot \varepsilon}, \quad (1)$$

where $N^{t\bar{t}}$ is the number of $t\bar{t}$ events from the fit, B the branching fraction for the e +jets (μ +jets) final state where the e (μ) is allowed to originate from $W \rightarrow e$ ($W \rightarrow \mu$) or $W \rightarrow \tau \rightarrow e$ ($W \rightarrow \tau \rightarrow \mu$), \mathcal{L} the integrated luminosity and ε the preselection efficiency.

source	e +jets	μ +jets	combination
primary vertex id	± 0.16	$+0.18 / - 0.17$	$+0.17 / - 0.16$
lepton id	$+0.35 / - 0.38$	$+0.47 / - 0.42$	± 0.28
jet energy scale	$+0.14 / - 0.15$	$+0.00 / - 0.10$	$+0.08 / - 0.04$
jet id	± 0.01	$-0.01 / - 0.01$	± 0.01
jet resolution	$+0.01 / - 0.05$	$+0.17 / - 0.08$	$+0.02 / - 0.05$
trigger efficiencies	$+0.03 / - 0.06$	$+0.14 / - 0.16$	± 0.1
multijet background	± 0.04	$+0.08 / - 0.06$	± 0.05
W +jets simulation	± 0.53	± 0.48	± 0.51
template statistics	± 0.34	± 0.43	± 0.27
other	± 0.13	± 0.12	± 0.13
total	± 0.8	$+0.9 / - 0.8$	± 0.7

TABLE V: Summary of the systematic uncertainties on the top-antitop quark pair production cross section in pb.

The result of the $t\bar{t}$ production cross section in the e +jets and the μ +jets channel at $\sqrt{s}=1.96$ TeV for a top mass of 175 GeV/ c^2 yields respectively:

$$\begin{aligned}\sigma_{p\bar{p}\rightarrow t\bar{t}+X} &= 6.6_{-1.1}^{+1.2} (\text{stat}) \pm 0.8 (\text{syst}) \pm 0.4 (\text{lumi}) \text{ pb} \quad (\text{in the } e\text{-jets channel}), \\ \sigma_{p\bar{p}\rightarrow t\bar{t}+X} &= 5.9_{-1.2}^{+1.3} (\text{stat})_{-0.8}^{+0.9} (\text{syst}) \pm 0.4 (\text{lumi}) \text{ pb} \quad (\text{in the } \mu\text{-jets channel}).\end{aligned}$$

The combination of the two results, taking into account the correlation of systematic uncertainties, yields:

$$\sigma_{p\bar{p}\rightarrow t\bar{t}+X} = 6.3_{-0.8}^{+0.9} (\text{stat}) \pm 0.7 (\text{syst}) \pm 0.4 (\text{lumi}) \text{ pb}.$$

Figure 7 shows the discriminant distribution in lepton+jets data with the fitted fractions of the signal, W +jets and multijet background. Figure 8 shows the distributions of likelihood input variables for data overlaid with the predicted distributions from the simulation. Distributions of the kinematic variables not used in the discriminant are presented in Figure 9. Figure 10 displays lepton p_T distributions in data overlaid with the signal and background model prediction for the events dominated by the background (signal) with discriminant below (above) 0.5.

We find that all measurements are in good agreement with the Standard Model prediction and with each other.

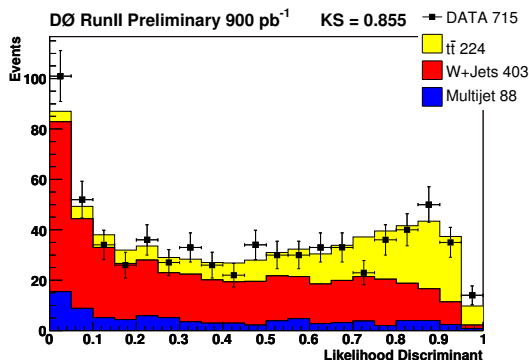


FIG. 7: Likelihood discriminant distribution for data overlaid with the result from the fit of top-antitop quark pair production, W +jets production and multijet background templates for ℓ +jets events.

Acknowledgements

We thank the staffs at Fermilab and collaborating institutions, and acknowledge support from the DOE and NSF (USA); CEA and CNRS/IN2P3 (France); FASI, Rosatom and RFBR (Russia); CAPES, CNPq, FAPERJ, FAPESP and FUNDUNESP (Brazil); DAE and DST (India); Colciencias (Colombia); CONACyT (Mexico); KRF and KOSEF (Korea); CONICET and UBACyT (Argentina); FOM (The Netherlands); PPARC (United Kingdom); MSMT (Czech Republic); CRC Program, CFI, NSERC and WestGrid Project (Canada); BMBF and DFG (Germany); SFI (Ireland);

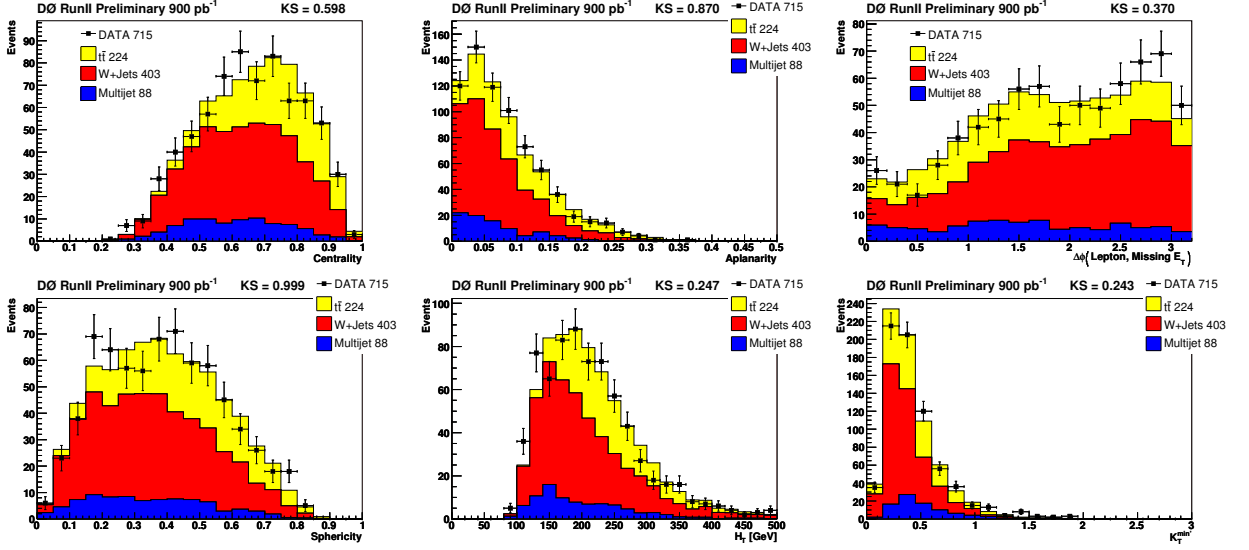


FIG. 8: Likelihood discriminant input distributions in the data overlaid with the prediction from simulation and multijet background data for ℓ +jets events.

The Swedish Research Council (Sweden); Research Corporation; Alexander von Humboldt Foundation; and the Marie Curie Program.

-
- [1] N. Kidonakis and R. Vogt, Phys. Rev. D **68**, 114014 (2003).
 [2] M. Cacciari, S. Frixione, G. Ridolfi, M. Mangano, P. Nason, JHEP 404, 68 (2004).
 [3] DØ Collaboration, V.M. Abazov *et al.*, Nucl. Instrum. and Methods A **565**, 463 (2006).
 [4] DØ Collaboration, S. Abachi *et al.*, Nucl. Instrum. Methods Phys. Res. A **338**, 185 (1994).
 [5] G. Blazey *et al.*, “Run II Jet Physics”, hep-ex/0005012.
 [6] The normalized momentum tensor \mathcal{M} is defined as:

$$\mathcal{M}_{ij} = \frac{\sum_o p_i^o p_j^o}{\sum_o |\vec{p}^o|^2},$$

where \vec{p}^o is the momentum-vector of a reconstructed object o , and i and j are Cartesian coordinates. \mathcal{M}_{ij} has three eigenvalues $\lambda_1 \geq \lambda_2 \geq \lambda_3$, with $\lambda_1 + \lambda_2 + \lambda_3 = 1$. The objects included in the sum are the jets and the charged lepton from the W boson decay.

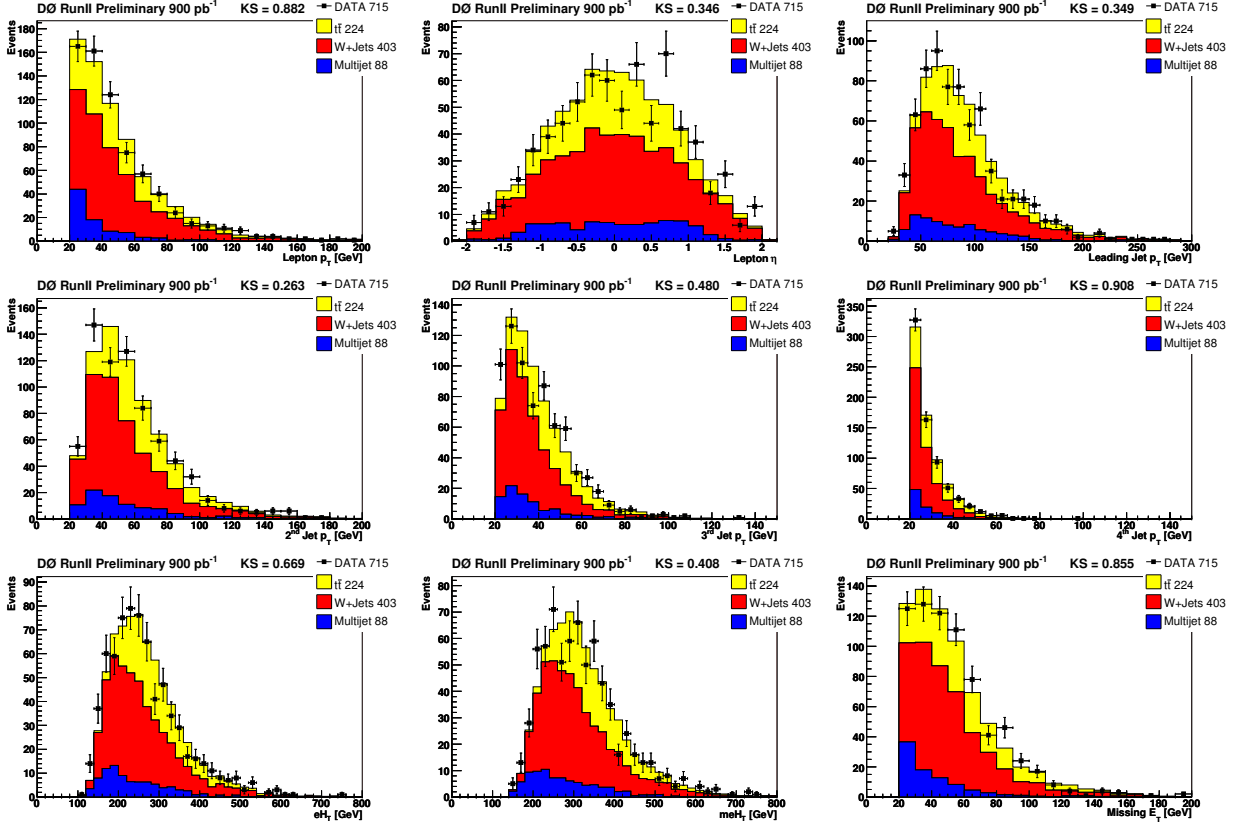


FIG. 9: Distributions of kinematic variables not used in the discriminant for the data overlaid with the prediction from simulation and multijet background data for ℓ +jets events. For the eH_T (meH_T) variable, in addition to the jets the lepton p_T (and \cancel{E}_T) has been used when calculating H_T .

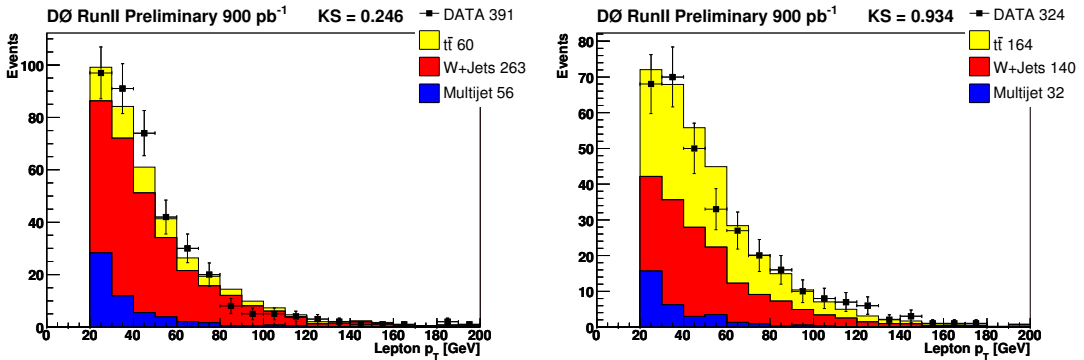


FIG. 10: Lepton p_T distribution in the data overlaid with the prediction from simulation and multijet background data for ℓ +jets events, using events with the discriminant less than 0.5 (left) and more than 0.5 (right).

APPENDIX A: CONTROL PLOTS FOR INDIVIDUAL CHANNELS

Figures 11 and 12 show the distributions of likelihood input variables for data overlaid with the predicted distributions from the simulation. Kolmogorov-Smirnov (KS) probabilities are given in upper center of each plot to quantify the agreement between the observed and predicted distributions.

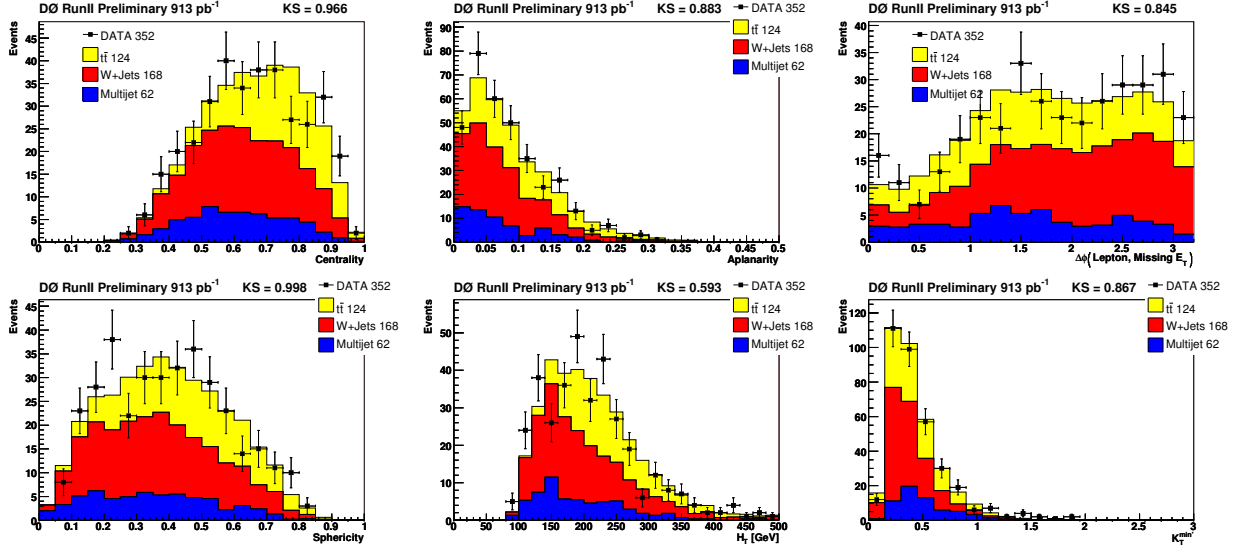


FIG. 11: Likelihood discriminant input distributions for the data overlaid with the prediction from simulation and multijet background data for e +jets events.

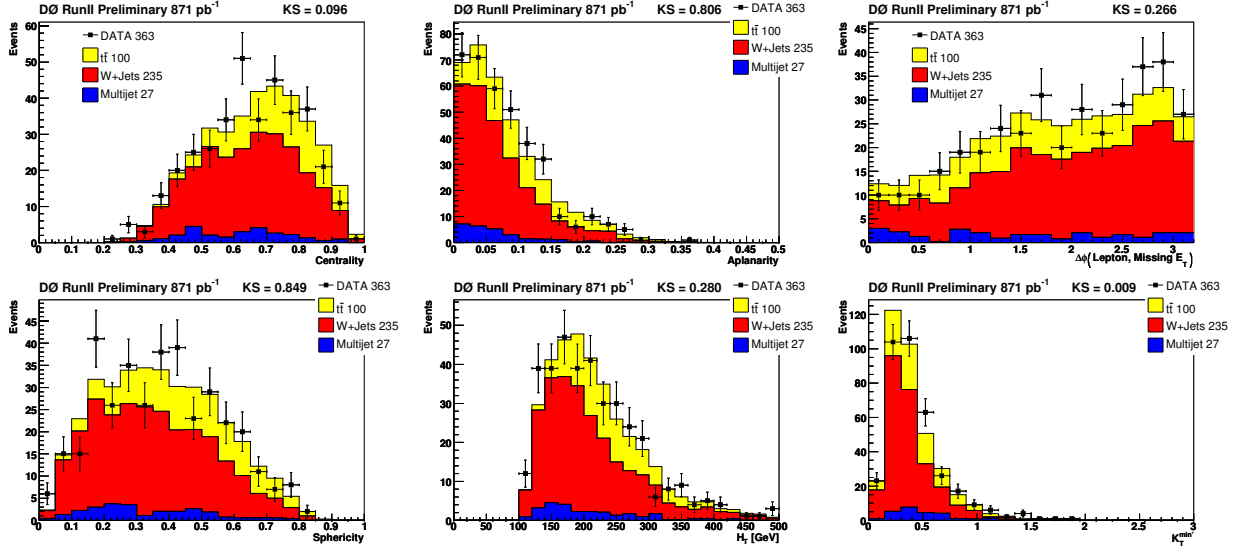


FIG. 12: Likelihood discriminant input distributions for the data overlaid with the prediction from simulation and multijet background data for μ +jets events.